Biochemical and Biophysical Research Communications 409 (2011) 622–627

Contents lists available at ScienceDirect

Biochemical and Biophysical Research Communications

journal homepage: www.elsevier.com/locate/ybbrc

# Structure of a novel class II phospholipase D: Catalytic cleft is modified by a disulphide bridge

Priscila Oliveira de Giuseppe [a,1], Anwar Ullah [b,1], Dilza Trevisan Silva [c], Luiza Helena Gremski [c], Ana Carolina Martins Wille [c,d], Daniele Chaves Moreira [c], Andrea Senff Ribeiro [c], Olga Meiri Chaim [c], Mario Tyago Murakami [a], Silvio Sanches Veiga [c], Raghuvir Krishnaswamy Arni [b,*]

[a] Laboratório Nacional de Biociências (LNBio), Centro Nacional de Pesquisa em Energia e Materiais, Campinas, 13083-970 SP, Brazil
[b] Centro Multiusuário de Inovação Biomolecular, Departamento de Física, Universidade Estadual Paulista (UNESP), São José do Rio Preto, 15054-000 SP, Brazil
[c] Departamento de Biologia Celular, Universidade Federal do Paraná, Curitiba, 80060-000 PR, Brazil
[d] Department of Structural, Molecular Biology and Genetics, State University of Ponta Grossa, Ponta Grossa, Paraná, Brazil

ARTICLE INFO

*Article history:*
Received 22 April 2011
Available online 17 May 2011

*Keywords:*
Loxosceles spider venom
Phospholipase D
Crystal structure

ABSTRACT

Phospholipases D (PLDs) are principally responsible for the local and systemic effects of *Loxosceles* envenomation including dermonecrosis and hemolysis. Despite their clinical relevance in loxoscelism, to date, only the SMase I from *Loxosceles laeta*, a class I member, has been structurally characterized. The crystal structure of a class II member from *Loxosceles intermedia* venom has been determined at 1.7 Å resolution. Structural comparison to the class I member showed that the presence of an additional disulphide bridge which links the catalytic loop to the flexible loop significantly changes the volume and shape of the catalytic cleft. An examination of the crystal structures of PLD homologues in the presence of low molecular weight compounds at their active sites suggests the existence of a ligand-dependent rotamer conformation of the highly conserved residue Trp230 (equivalent to Trp192 in the glycerophosphodiester phosphodiesterase from *Thermus thermophofilus*, PDB code: 1VD6) indicating its role in substrate binding in both enzymes. Sequence and structural analyses suggest that the reduced sphingomyelinase activity observed in some class IIb PLDs is probably due to point mutations which lead to a different substrate preference.



## 1. Introduction

Envenomation by brown spiders (*Loxosceles* spp.) leads to a strong local dermonecrotic effect (cutaneous loxoscelism) and systemic manifestations, whose symptoms include hematuria, hemoglobinuria, jaundice and fever [1–3]. Although, the systemic loxoscelism occurs in a minority of cases, it can be fatal, especially in children [1–3].

Phospholipases D (PLD) are considered the main components responsible for the local and systemic effects of *Loxosceles* venom including dermonecrosis, renal toxicity and hemolysis [4–9]. *Loxosceles* PLDs (30–35 kDa), also referred to as dermonecrotic toxins, were primarily designated as sphingomyelinases D (SMases D) due to their ability to convert sphingomyelin to choline and ceramide 1-phosphate (*N*-acylsphingosine1-phosphate) [4]. As some *Loxosceles* PLDs have broad substrate specificity, being able to hydrolyze not only sphingophospholipids but also lysoglycerophospholipids, they are now classified as phospholipases D [10–12].

PLDs can be grouped into two classes based on sequence, structural and biochemical data [13]. The class I, represented by PLD I from *Loxosceles laeta*, is characterized by the presence of a single disulphide bridge (Cys51–Cys57) and an extended hydrophobic loop (variable loop). Class II comprises PLDs that contain an additional intra-chain disulphide bridge linking the flexible loop and the catalytic loop. Depending on their ability to hydrolyze sphingomyelin, they are further subdivided into classes IIa (more active) and IIb (less active or inactive), respectively [13].

Despite the clinical importance of these enzymes in loxoscelism, to date, only the PLD I from *L. laeta*, a class I member, had been structurally characterized [14]. Based on its crystal structure, an acid–base catalytic mechanism was proposed, where His12 and His47 play key roles and are supported by a network of hydrogen bonds between Asp34, Asp52, Trp230, Asp233, and Asn252 [14]. However, the vast majority of *Loxosceles* PLDs belongs to the class II, and none of their three-dimensional structures have been determined. A representative member of class II PLD is the dermonecrotic toxin isoform 1 from *Loxosceles intermedia* [11]. The recombinant protein

* Corresponding author.
*E-mail address:* arni@ibilce.unesp.br (R.K. Arni).
[1] Both authors have contributed equally to this work.

0006-291X/$ - see front matter © 2011 Elsevier Inc. All rights reserved.
doi:10.1016/j.bbrc.2011.05.053

(LiRecDT1) is able to hydrolyze sphingomyelin and presents dermonecrotic and hemolytic activities, characteristics of the whole venom [10,11,15,16]. Moreover, LiRecDT1 is able to directly induce renal injuries in mice and its nephrotoxic effects are dependent on its catalytic activity [11]. It has also been demonstrated that LiRecDT1 released choline from endothelial and kidney cell membrane extracts and bound to various lipids, such as sphingomyelin, lysophosphatidylcholine and cholesterol [12].

This work presents the first crystal structure of a *Loxosceles* venom class II PLD, the dermonecrotic toxin isoform 1 from *L. intermedia*. A comparison of the three-dimensional structures of class I and II PLDs, indicates the effect of an additional disulfide bridge which links the surface loops on the volume and shape of the catalytic cleft. Sequence and structural analyses suggest that the reduced or absent sphingomyelinase activity of some class IIb PLDs [15,17,18] is probably due to mutations of amino acid residues affecting substrate affinity or protein stability, since all catalytically-relevant residues are fully conserved. Moreover, the mutations observed at the catalytic pocket of these proteins are the same encountered in the active PLD 2 from *L. laeta* [19].

## 2. Materials and methods

### 2.1. Expression and purification

Mature dermonecrotic toxin isoform 1 from *L. intermedia* (LiRecDT1) was cloned into a pET-14b vector (Novagen, Madison, USA) and expressed in *Escherichia coli* BL21(DE3)pLysS cells (Invitrogen) as described previously [20]. Expression was induced by the addition of 0.05 mM IPTG (isopropyl β-D-thiogalactoside) during 3.5 h at 303 K after the cell culture had reached an $OD_{550}$ of 0.5.

Cell suspension was disrupted by six 10 s-cycles of sonication. Lysed material was centrifuged (20,000*g*, 20 min) and the supernatant was incubated with 1 ml $Ni^{2+}$-NTA agarose beads for 1 h at 277 K. The suspensions were loaded onto a column and the packed gel was washed with 50 mM sodium phosphate pH 8.0, 500 mM NaCl, 20 mM imidazole. The recombinant protein was eluted with 10 ml of the above buffer which additionally contained 250 mM imidazole and 1 ml fractions were collected and analyzed by 12.5% SDS–PAGE. Fractions were pooled and dialyzed against phosphate buffer saline (PBS).

### 2.2. Crystallization

The LiRecDT1 protein was crystallized by vapor diffusion in sitting drops using a Cartesian HoneyBee 963 system (Genomic Solutions) at 291 K as described in [20]. Optimal crystals were observed in drops containing 2 μl of the protein solution (17 mg $ml^{-1}$) and 2 μl of the reservoir solution equilibrated over 1 ml of reservoir solution (0.1 M Tris–HCl pH 7.5, 40% (v/v) PEG200).

### 2.3. Data collection and processing

LiRecDT1 crystals were directly flash-cooled in a 100 K nitrogen-gas stream. X-ray diffraction data were collected on the W01B-MX2 beamline at the Brazilian Synchrotron Light Laboratory (Campinas, Brazil) as described in earlier [20]. The data were indexed, integrated and scaled using the DENZO and SCALEPACK programs from the HKL-2000 package [21]. Data collection and refinement statistics are summarized in Table 1.

### 2.4. Structure solution and refinement

The initial structural model of LiRecDT1 was determined by molecular-replacement using the program MOLREP [22] and the atomic coordinates of PLD 1 from *L. laeta* as the template (PDB code 1XX1; [14]). Model refinement was carried out alternating cycles of REFMAC5 [23] with visual inspection of the electron density maps and manual rebuilding with COOT [24]. A total of 278 residues were modeled, comprising LiRecDT1 residues from Gly2 to Lys284, numbered according to the class I phospholipase D structure (PDB code 1XX1; [14]). Water molecules were added using COOT [24] during the last refinement cycles. One magnesium ion ($Mg^{2+}$), two ethylene glycol (EDO), four diethylene glycol (PEG) and one triethylene glycol (PGE) were modeled based on the difference Fourier map of LiRecDT1. The final model consists of one monomer and was established after the convergence of $R_{factor}$ and $R_{free}$ values to 17.2% and 21.4%, respectively. Analyses of monomer–monomer interfaces using the PISA web server [25] did not indicate any biologically relevant quaternary structure in the crystal. Stereochemistry of the model was analyzed with Molprobity [26]. No outlier was observed in the Molprobity Ramachandran plot and more than 99% of the residues are in its favored region. Data collection and structure refinement statistics are summarized in Table 1. Figures were produced using the program Pymol [27].

**Table 1**
Data collection and refinement statistics.

| *Data collection*[a] | |
|---|---|
| Temperature (K) | 100 |
| Radiation source | W01B-MX2 (LNLS, Brazil) |
| Wavelength (Å) | 1.458 |
| Detector | MarMosaic 225 |
| Space group | $P12_11$ |
| Unit-cell parameters (Å, °) | $a$ = 49.81, $b$ = 49.30 and $c$ = 56.30; $\beta$ = 105.83 |
| Resolution range (Å) | 24.65–1.72 (1.81–1.72) |
| $R_{merge}$[b] (%) | 9.7 (46.8) |
| $\langle I/\sigma(I)\rangle$ | 8.1 (2.0) |
| Data completeness (%) | 99.9 (99.9) |
| No. of measured reflections | 102,021 (14,085) |
| No. of unique reflections | 28,041 (4040) |
| Multiplicity | 3.6 (3.5) |
| *Structure refinement statistics* | |
| $R_{factor}$ | 17.2 |
| $R_{free}$ | 21.4 |
| r.m.s.d. Bond distances (Å) | 0.023 |
| r.m.s.d. Bond angles (°) | 1.930 |
| Ramachandran outliers (%) | 0 |
| Ramachandran favored (%) | 99.3 |
| Average *B*-factors (Å$^2$) | 17.74 |

[a] Values in parentheses are for the last resolution shell.
[b] $R_{merge} = \sum_{hkl}\sum_i|I_i(hkl) - \langle I(hkl)\rangle|/\sum_{hkl}\sum_i I_i(hkl)$, where $I_i(hkl)$ is the $i$th observation of reflection $hkl$ and $\langle I(hkl)\rangle$ is the weighted average intensity for all observations $I$ of reflection $hkl$.

### 2.5. Molecular modeling and quality analysis

The atomic coordinates of LiRecDT1 (PDB code: 3RLH) was used as the initial model to obtain three-dimensional models of LiRecDT3 from *L. intermedia* (ABB71184.1) and Lb3 from *L. boneti* (AAT66074.1), using the modeling option of the Swiss-Model server [28]. For energy minimization, the final models were submitted under explicit solvent molecular dynamics (MD) simulations using YASARA until the convergence of root mean square deviation (r.m.s.d.) (Fig. S1). The overall and local quality analysis of the final model was assessed by ProSA-web [29] and Molprobity [26]. More than 99% of the residues of both models are in the favored region of the Ramachandran plot. ProSA-web analyses indicated that the referred models present *Z*-scores within the range typically observed for native proteins of similar size.

## 3. Results and discussion

### 3.1. Overall structure

LiRecDT1 is a single domain protein which folds into a TIM $(\alpha/\beta)_8$-barrel with the insertion of additional β-strands and α-helices (Fig. 1). FastSCOP [30] analysis indicates that this class II PLD belongs to the phospholipase C (PLC) like phosphodiesterases superfamily, suggesting that PLDs share a common ancestor with PLC like domains encountered in mammalian phospholipase C isozyme D1 [30], bacterial phosphatidylinositol-specific phospholipase C [31] and glycerophosphodiester phosphodiesterases [32].

The catalytic (blue), variable (green), flexible (red) and other short loops surround the active site cleft (Fig. 1). The catalytic loop, which contains the catalytically important residue, His47, forms a hairpin due to the presence of a disulphide bridge (Cys51–Cys57). A network of hydrogen bonds ensures the correct relative orientation of the hairpin in relation to the core of the protein.

### 3.2. Structural comparison between class I and II phospholipases D

LiRecDT1 superimposes on the class I PLD from *L. laeta* (SMase I) (PDB code: 1XX1; [19]) with a r.m.s. deviation of 0.938 Å for 268 Cα atoms and a sequence identity of 61.6 %. The main conformational changes are observed at the flexible and variable loops (Fig. 1). LiRecDT1 possesses a disulfide bridge between Cys53 and Cys201, which causes a large displacement of the flexible loop towards the catalytic loop (Fig. 1). This disulfide bridge is well conserved in class II PLDs, but absent in class I PLD due to the mutation C201F (Fig. 2).

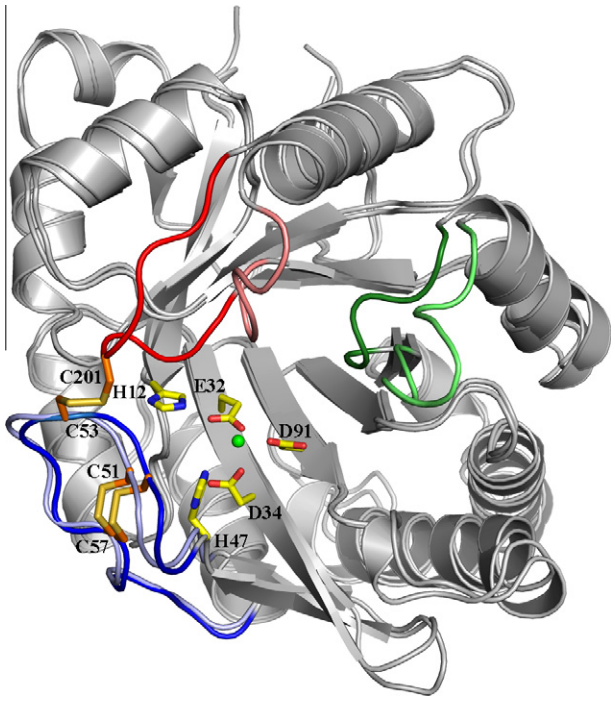


**Fig. 1.** Structural alignment between LiRecDT1 (class II) and PLD I from *L. laeta* (class I). The LiRecDT1 residues involved in metal–ion binding and catalysis are presented in atom colors (PDB code: 3RLH). The $Mg^{2+}$ ion is shown as a green sphere. The catalytic, flexible, and variable loops are colored in blue, red, and green, respectively. Dark and light colors refer to LiRecDT1 and *L. laeta* PLD, respectively. The disulphide bridges are presented by orange sticks. (For interpretation of the references to colour in this figure legend, the reader is referred to the web version of this article.)

Regarding the variable loop, a five-residue insertion (YLPSL), which protrudes from the core structure of class I PLD, is absent in the class II PLD (Figs. 1 and 2). Moreover, the three last residues that compose the variable loop are not conserved between class I and class II PLDs (Fig. 2). The mean *B*-factors for the main-chain atoms of the variable loops are 26.39 $Å^2$ and 15.86 $Å^2$ for class I (PDB code: 1XX1, chain A) and class II respectively, indicating that the class I variable loop is significantly more flexible than that of class II.

In the class II PLD, the flexible loop is displaced towards the catalytic loop and partially occludes an electronegative cleft that leads to the active site in the class I PLD (Fig. 3). This results in a volumetric reduction of the cavity that forms the catalytic site of the class II PLD. Based on SURFNET analysis [33], the volume and average depth of the cleft observed at the class I PLD catalytic face are 4339.4 $Å^3$ and 15.2 Å, respectively. These values are considerably larger than those estimated for the corresponding cavity at the class II PLD (volume 1468.1 $Å^3$, average depth 10.1 Å). Besides the lack of the disulfide bridge connecting the catalytic and flexible loops, the protrusion of variable loop and the substitution N137G also account for the enlargement of the cleft surrounding the catalytic site of the class I PLD (Fig. 3).

A large electronegative patch, which includes the variable loop, is observed surrounding the right side of the class II PLD catalytic pocket. However, in the class I PLD, this patch is interrupted by the longer variable loop that forms a protrusion with neutral potential (Fig. 3). Interestingly, an electronegative cleft, hidden by the neutral catalytic and flexible loops in the class II PLD, is exposed in the class I PLD, due to the absence of a disulfide bridge connecting these loops. Thus, in the class I PLD the impairment in the electronegative potential of a patch at the right side of the catalytic pocket seems to be compensated by the exposure of another electronegative patch on the left side.

Together, these differences observed in the topography and electrostatic potential distribution of class I and II PLDs catalytic faces suggest that these enzymes might have different ways to guide the substrate into the catalytic pocket.

### 3.3. Active site

The $Mg^{2+}$ binding site and the two catalytic histidine residues (His12 and His47), which compose the active-site pocket are strictly conserved in both classes of spider venom PLDs (Fig. 2). Interestingly, at the active site of LiRecDT1, the difference Fourier map contained residual density. However, neither substrates nor products could account for this density. This residual density was modeled as two PEG molecules with partial occupancy.

In the LiRecDT1 structure, the $Mg^{2+}$ ion (B factor of 14.26 $Å^2$ and a mean Mg–O bond distance of 2.1 Å) is hexacoordinated by the carboxyl oxygens of Glu32, Asp34, Asp91, one water molecule and two PEG4 oxygens. The same geometric coordination is observed for the $Mg^{2+}$ ion in class I PLD structure bound to a sulfate ion [13]. As pointed out earlier, *Loxosceles* PLDs and glycerophosphodiester phosphodiesterases (GDPDs) share a similar divalent metal dependent catalytic mechanism and probably evolved from a common ancestor [14]. In spite of their different specificities, structural comparisons of the PLD and GDPD active sites suggest that they share not only residues involved in metal binding and catalysis but also in substrate binding such as Lys93 and Trp230 (Fig. 4A). Murakami et al. have suggested a role for Lys93 and Trp230 in the orientation of the substrate in both spider and bacterial PLDs [14]. Structural analysis indicates that the Lys residue might interact with the phosphate moiety of GDPDs substrates. Moreover, since the mutation K121A greatly reduces the enzymatic activity of the *Thermoanaerobacter tengcongensis* GDPD, suggesting that this Lys residue affects catalysis via electronic

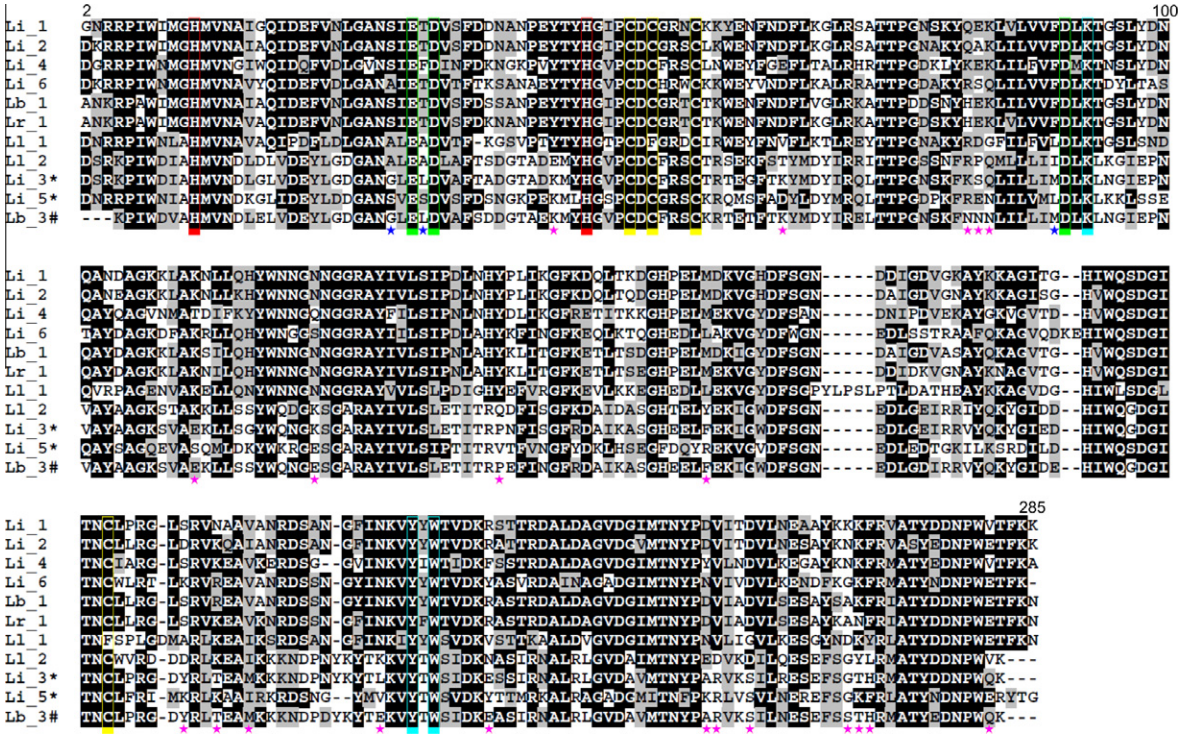

**Fig. 2.** Multiple sequence alignment of class I and II PLDs. Li_1 (LiRecDT1, PDB code: 3RLH), Li_2 (LiRecDT2, ABB69098.1), Li_3 (LiRecDT3, ABB71184.1), Li_4 (LiRecDT4, ABD91846.1), Li_5 (LiRecDT5, ABD91847.1) and Li_6 (LiRecDT6, ABO87656.1) are PLDs paralogs from *L. intermedia*. Ll_1 (AAM21154.1, PDB code: 1XX1) and Ll_2 (AAM21156.1) are isoforms from *L. laeta*, Lb_1 (AAT66073.1) and Lb_3 (AAT66074.1) are PLDs from *L. boneti* and Lr_1 (AAT66075.1) is a PLD from *L. reclusa*. The symbols ∗ and # indicate PLDs with reduced or abolished sphingomyelinase activity, respectively. Residues involved in metal–ion binding and catalysis are boxed in green and red, while cysteines are boxed in yellow. Residues possibly involved in substrate binding and orientation are boxed in cyan. The numbers represent the class I PLD sequence. Stars indicate amino acid substitutions occurred specifically in PLDs with reduced or abolished sphingomyelinase activity. Blue stars refer to buried residues near to the metal-binding site and pink stars refer to surface-exposed residues. (For interpretation of the references to colour in this figure legend, the reader is referred to the web version of this article.)

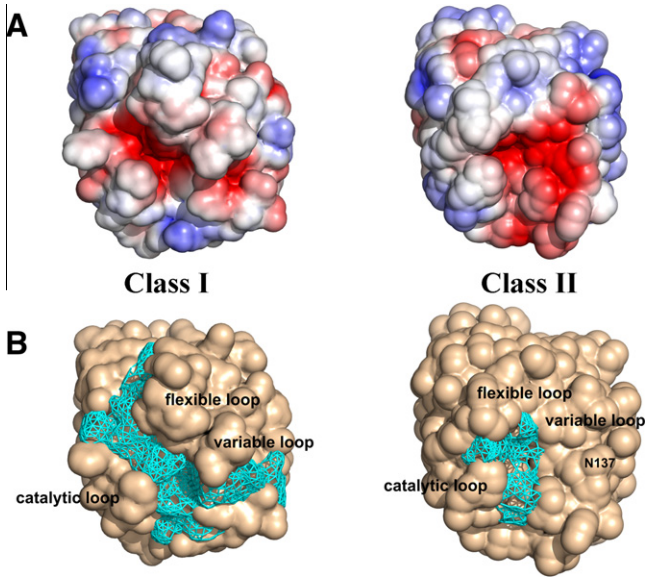


**Fig. 3.** Solvent accessible surface analyses of class I and II PLDs. (A) Electrostatic surface of class I (left) and II (right) PLDs are colored by charge, from red (−2 kV) to blue (+2 kV). Electrostatic potential was calculated using PBEQ solver [38]. (B) Representation of the largest cavities (*cyan*) in the respective class I and II PLD structures. Models are oriented according to Fig. 1. Class I PLD = PDB code: 1XX1, chain A. Class II PLD = PDB code: 3RLH. (For interpretation of the references to colour in this figure legend, the reader is referred to the web version of this article.)

interaction with the phosphate moiety of the substrate [34]. A similar role might be attributed to the corresponding Lys residue in spider PLDs.

Trp230, strategically located at the bottom of the active site, adopts different rotamer conformations depending on the presence of ligands (Fig. 4B and C). The equivalent in the GDPD from *Thermus thermophofilus* is Trp192 (PDB code: 1VD6). In the presence of PEG (PDB code: 3RLH) or glycerol (PDB code: 1VD6) molecules, Trp230(192) forms one of the walls of the active site pocket, freeing space for ligand binding. The presence of a sulfate ion in the active site of class I PLD (PDB code: 1XX1) induces another conformation of Trp230 by the formation of a hydrogen bond between the NE1 nitrogen of Trp230 and the sulfate O1 atom. Contrastingly, in the ligand free form of class I PLD (PDB code: 2F9R), the Trp230 ring adopts a third conformation in which the torsion angle $\chi 2$ changes by $-90°$ in relation to the Trp230 conformation in presence of PEG or glycerol. These findings suggest that Trp230 motions might play a pivotal role in substrate binding in both *Loxosceles* venom PLDs and bacterial GDPDs.

### 3.4. Functional diversification in spider venom PLDs

The spider venom PLDs encompass a gene family with multiple orthologs and paralogs, which differ in catalytic efficiency, substrate specificity or intensity of biological effects [7,10,11,15–19,35,36]. A structure-based classification segregates these enzymes into two major groups as mentioned in the introduction. This classification is in agreement with recent phylogenetic analysis of a large set of Sicariid spider venom PLDs, which grouped members of different classes into distinct branches belonging to

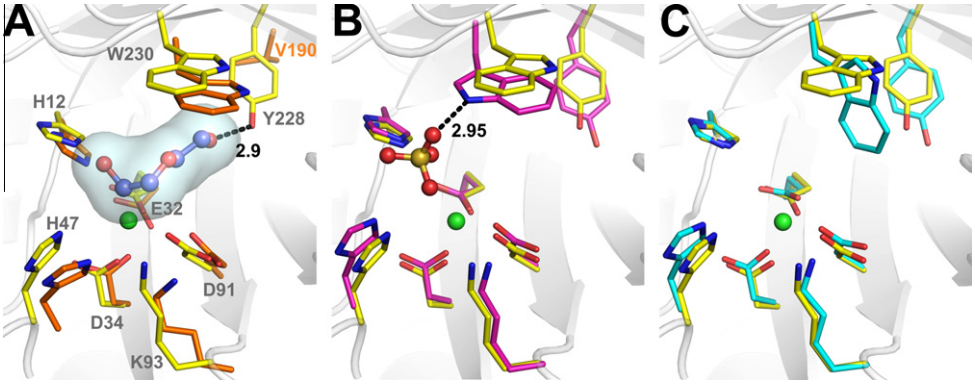


**Fig. 4.** The active site. Structural alignment among class I and II PLDs and a glycerophosphodiester phosphodiesterase (GDPD) from *Thermus thermophilus*. (A) Representation of class II PLD (carbon atoms in yellow) and GDPD (carbon atoms in orange C) superposed structures highlighting the PEG molecule (carbon atoms in violet) from the class II PLD structure. (B) Representation of class II PLD and class I PLD (carbon atoms in magenta) superposed structures showing the sulfate ion from the class I structure. (C) Representation of class II PLD and the sulfate-free class I (cyan C atoms) superposed structures. Nitrogen, oxygen, sulfur and magnesium atoms are colored blue, red, wheat and green, respectively. PDB codes: GDPD (1VD6:A), class I PLD (1XX1:D), sulfate free class I PLD (2F9R:B), class II PLD (3RLH). (For interpretation of the references to colour in this figure legend, the reader is referred to the web version of this article.)

two major clades (α and β). Clade α includes class I and IIa PLDs whereas clade β includes class IIb PLDs [36].

In an attempt to understand the structural determinants for the functional divergence of β clade members with reduced sphingomyelinase activity [15], we analyzed mutations exclusively observed in these enzymes (Fig. 2). Three of these mutations (S30G, T33L, F90M), are observed at the protein hydrophobic core and prediction of protein stability by the PoPMuSiC program [37] suggests that the substitutions S30G and F90M may have a destabilizing effect. The other substitutions are sparsely distributed on the LiRecDT1 surface relatively far from the catalytic pocket. Considering the long aliphatic tail of sphingomyelin, changes in the charge distribution and surface shape of the catalytic face induced by some of these mutations may affect the protein–lipid interaction and, consequently, their substrate affinity.

This analysis of the active site pockets in the structures of the class I, the class II and the modeled structure of Lb3 did not provide a clear explanation for the reduced or absent sphingomyelinase activity of LiRecDT3 and Lb3. These proteins conserve the $Mg^{2+}$ binding site residues along with Lys93, Tyr228, Trp230 and the two catalytic histidine residues (His12 and His47) (Fig. 2 and Fig. S2). Moreover, the substitutions observed at their catalytic site are the same encountered in the active Ll2 enzyme. This suggests that LiRecDT3, LiRecDT5 and Lb3 may not be devoid of catalytic activity but might possess affinity to other substrates. This hypothesis is supported by the fact that some spider venom PLDs demonstrates broad substrate selectivity [13–15].

## Acknowledgments

This work was supported by grants from Fundação de Amparo a Pesquisa do Estado de São Paulo (FAPESP), Secretaria de Estado de Ciência, Tecnologia e Ensino Superior (SETI) do Paraná, Fundação Araucária-PR, CNPq and CAPES, Brazil.

## Appendix A. Supplementary data

Supplementary data associated with this article can be found, in the online version, at doi:10.1016/j.bbrc.2011.05.053.

## References

[1] J.M. Futrell, Loxoscelism, Am. J. Med. Sci. 304 (1992) 261–267.
[2] H.H. Sams, C.A. Dunnick, M.L. Smith, L.E. King, Necrotic arachnidism, J. Am. Acad. Dermatol. 44 (2001) 561–573.
[3] P.H. da Silva, R.B. da Silveira, M.H. Appel, O.C. Mangili, W. Gremski, S.S. Veiga, Brown spiders and loxoscelism, Toxicon 44 (2004) 693–709.
[4] L.J. Forrester, J.T. Barrett, B.J. Campbell, Red blood cell lysis induced by the venom of the brown recluse spider: the role of sphingomyelinase D, Arch. Biochem. Biophys. 187 (1978) 355–365.
[5] G. Kurpiewski, L.J. Forrester, J.T. Barrett, B.J. Campbell, Platelet aggregation and sphingomyelinase D activity of a purified toxin from the venom of *Loxosceles reclusa*, Biochim. Biophys. Acta 678 (1981) 467–476.
[6] M.de F. Fernandes Pedrosa, I. de L.M. Junqueira de Azevedo, R.M. Gonçalves-de-Andrade, C.W. van den Berg, C.R.R. Ramos, P.L. Ho, et al., Molecular cloning and expression of a functional dermonecrotic and haemolytic factor from *Loxosceles laeta* venom, Biochem. Biophys. Res. Commun. 298 (2002) 638–645.
[7] E. Kalapothakis, M. Chatzaki, H. Gonçalves-Dornelas, C.S. de Castro, F.G. Silvestre, F.V. Laborne, et al., The Loxtox protein family in *Loxosceles intermedia* (Mello-Leitão) venom, Toxicon 50 (2007) 938–946.
[8] D. Chaves-Moreira, O.M. Chaim, Y.B. Sade, K.S. Paludo, L.H. Gremski, L. Donatti, et al., Identification of a direct hemolytic effect dependent on the catalytic activity induced by phospholipase-D (dermonecrotic toxin) from brown spider venom, J. Cell. Biochem. 107 (2009) 655–666.
[9] O.M. Chaim, Y.B. Sade, R.B. da Silveira, L. Toma, E. Kalapothakis, C. Chávez-Olórtegui, et al., Brown spider dermonecrotic toxin directly induces nephrotoxicity, Toxicol. Appl. Pharmacol. 211 (2006) 64–77.
[10] L.A. van Meeteren, F. Frederiks, B.N.G. Giepmans, M.F.F. Pedrosa, S.J. Billington, B.H. Jost, et al., Spider and bacterial sphingomyelinases d target cellular lysophosphatidic acid receptors by hydrolyzing lysophosphatidylcholine, J. Biol. Chem. 279 (2004) 10833–10836.
[11] S. Lee, K.R. Lynch, Brown recluse spider (*Loxosceles reclusa*) venom phospholipase D (PLD) generates lysophosphatidic acid (LPA), Biochem. J. 391 (2005) 317–323.
[12] O.M. Chaim, R.B. da Silveira, D. Trevisan-Silva, V.P. Ferrer, Y.B. Sade, M. Bóia-Ferreira, et al., Phospholipase-D activity and inflammatory response induced by brown spider dermonecrotic toxin: endothelial cell membrane phospholipids as targets for toxicity, Biochim. Biophys. Acta 1811 (2011) 84–96.
[13] M.T. Murakami, M.F. Fernandes-Pedrosa, S.A. de Andrade, A. Gabdoulkhakov, C. Betzel, D.V. Tambourgi, et al., Structural insights into the catalytic mechanism of sphingomyelinases D and evolutionary relationship to glycerophosphodiester phosphodiesterases, Biochem. Biophys. Res. Commun. 342 (2006) 323–329.
[14] M.T. Murakami, M.F. Fernandes-Pedrosa, D.V. Tambourgi, R.K. Arni, Structural basis for metal ion coordination and the catalytic mechanism of sphingomyelinases D, J. Biol. Chem. 280 (2005) 13658–13664.
[15] R.B. de Silveira, R.B. Pigozzo, O.M. Chaim, M.H. Appel, J.L. Dreyfuss, L. Toma, et al., Molecular cloning and functional characterization of two isoforms of dermonecrotic toxin from *Loxosceles intermedia* (brown spider) venom gland, Biochimie 88 (2006) 1241–1253.
[16] R.O.S. Ribeiro, O.M. Chaim, R.B. da Silveira, L.H. Gremski, Y.B. Sade, K.S. Paludo, et al., Biological and structural comparison of recombinant phospholipase D toxins from *Loxosceles intermedia* (brown spider) venom, Toxicon 50 (2007) 1162–1174.
[17] R.B. da Silveira, R.B. Pigozzo, O.M. Chaim, M.H. Appel, D.T. Silva, J.L. Dreyfuss, et al., Two novel dermonecrotic toxins LiRecDT4 and LiRecDT5 from Brown spider (*Loxosceles intermedia*) venom: from cloning to functional characterization, Biochimie 89 (2007) 289–300.
[18] M.H. Appel, R.B. da Silveira, O.M. Chaim, K.S. Paludo, D.T. Silva, D.M. Chaves, et al., Identification, cloning and functional characterization of a novel dermonecrotic toxin (phospholipase D) from brown spider (*Loxosceles intermedia*) venom, Biochim. Biophys. Acta 1780 (2008) 167–178.

[19] G.I. de Santi Ferrara, M.deF. Fernandes-Pedrosa, I. de L.M. Junqueira-de-Azevedo, R.M. Gonçalves-de-Andrade, F.C.V. Portaro, D. Manzoni-de-Almeida, et al., SMase II, a new sphingomyelinase D from *Loxosceles laeta* venom gland: molecular cloning, expression, function and structural analysis, Toxicon 53 (2009) 743–753.
[20] A. Ullah, P.O. de Giuseppe, M.T. Murakami, D. Trevisan-Silva, A.C.M. Wille, D. Chaves-Moreira, et al., Crystallization and preliminary X-ray diffraction analysis of a class II phospholipase D from *Loxosceles intermedia* venom, Acta Crystallogr. F67 (2011) 234–236.
[21] Z. Otwinowski, W. Minor, Processing of X-ray diffraction data collected in oscillation mode, in: Macromolecular Crystallography Part A, Academic Press, 1997. pp. 307–326.
[22] A. Vagin, A. Teplyakov, MOLREP: an automated program for molecular replacement, J. Appl. Crystallogr. 30 (1997) 1022–1025.
[23] G.N. Murshudov, A.A. Vagin, E.J. Dodson, Refinement of macromolecular structures by the maximum-likelihood method, Acta Crystallogr. D53 (1997) 240–255.
[24] P. Emsley, K. Cowtan, Coot: model-building tools for molecular graphics, Acta Crystallogr. D60 (2004) 2126–2132.
[25] E. Krissinel, K. Henrick, Inference of macromolecular assemblies from crystalline state, J. Mol. Biol. 372 (2007) 774–797.
[26] V.B. Chen, W.B. Arendall, J.J. Headd, D.A. Keedy, R.M. Immormino, G.J. Kapral, et al., MolProbity: all-atom structure validation for macromolecular crystallography, Acta Crystallogr. D66 (2010) 12–21.
[27] W.L. DeLano, The PyMOL Molecular Graphics System, DeLano Scientific, San Carlos, CA, USA, (2002).
[28] T. Schwede, J. Kopp, N. Guex, M.C. Peitsch, SWISS-MODEL: an automated protein homology-modeling server, Nucleic Acids Res. 31 (2003) 3381–3385.
[29] M. Wiederstein, M.J. Sippl, ProSA-web: interactive web service for the recognition of errors in three-dimensional structures of proteins, Nucleic Acids Res. 35 (2007) W407–W410.
[30] J.A. Grobler, L.-O. Essen, R.L. Williams, J.H. Hurley, C2 domain conformational changes in phospholipase C-[delta]1, Nat. Struct. Mol. Biol. 3 (1996) 788–795.
[31] C.S. Gässler, M. Ryan, T. Liu, O.H. Griffith, D.W. Heinz, Probing the roles of active site residues in phosphatidylinositol-specific phospholipase C from *Bacillus cereus* by site-directed mutagenesis, Biochemistry 36 (1997) 12802–12813.
[32] K.N. Rao, J.B. Bonanno, S.K. Burley, S. Swaminathan, Crystal structure of glycerophosphodiester phosphodiesterase from *Agrobacterium tumefaciens* by SAD with a large asymmetric unit, Proteins 65 (2006) 514–518.
[33] R.A. Laskowski, SURFNET: a program for visualizing molecular surfaces, cavities, and intermolecular interactions, J. Mol. Graph. 13 (1995) 323–330.
[34] L. Shi, J.F. Liu, X.-M. An, D.C. Liang, Crystal structure of glycerophosphodiester phosphodiesterase (GDPD) from *Thermoanaerobacter tengcongensis*, a metal ion-dependent enzyme: insight into the catalytic mechanism, Proteins 72 (2008) 280–288.
[35] S.A. de Andrade, M.T. Murakami, D.P. Cavalcante, R.K. Arni, D.V. Tambourgi, Kinetic and mechanistic characterization of the Sphingomyelinases D from *Loxosceles intermedia* spider venom, Toxicon 47 (2006) 380–386.
[36] G.J. Binford, M.R. Bodner, M.H.J. Cordes, K.L. Baldwin, M.R. Rynerson, S.N. Burns, et al., Molecular evolution, functional variation, and proposed nomenclature of the gene family that includes sphingomyelinase D in sicariid spider venoms, Mol. Biol. Evol. 26 (2009) 547–566.
[37] Y. Dehouck, A. Grosfils, B. Folch, D. Gilis, P. Bogaerts, M. Rooman, Fast and accurate predictions of protein stability changes upon mutations using statistical potentials and neural networks: PoPMuSiC-2.0, Bioinformatics 25 (2009) 2537–2543.
[38] S. Jo, M. Vargyas, J. Vasko-Szedlar, B. Roux, W. Im, PBEQ-solver for online visualization of electrostatic potential of biomolecules, Nucleic Acids Res. 36 (2008) W270–W275.